Title

Swelling and Diffusion during Methanol Sorption into Hydrated Nafion

Journal

The Journal of Physical Chemistry B, 122(34)

ISSN

1520-6106

Authors

Soniat, Marielle

Houle, Frances A

Publication Date

2018-08-30

DOI

10.1021/acs.jpcb.8b03169

Peer reviewed

Swelling and Diffusion during Methanol Sorption into Hydrated Nafion

*Marielle Soniat and Frances A. Houle**

Joint Center for Artificial Photosynthesis, Lawrence Berkeley National Laboratory, Berkeley, CA 94720; Chemical Sciences Division, Lawrence Berkeley National Laboratory, Berkeley, CA 94720

Abstract

Diffusion within polymer electrolyte membranes is often coincident with time-dependent processes such as swelling and polymer relaxation, which are factors that limit their ability to block molecular cross-over during use. The solution-diffusion model of membrane permeation, which is the accepted theory for dense polymers, applies only to steady-state processes and does not address dynamic internal structural changes that can accompany permeation. To begin discovery of how such changes can be coupled to the permeation process, we have constructed a stochastic multi-scale reaction-diffusion model that examines time-dependent methanol uptake into and swelling of hydrated Nafion. Several potential mechanisms of diffusion and polymer response are tested. The simulation predictions are compared to real-time Fourier transform infrared attenuated total reflectance spectroscopy (FTIR-ATR) absorbance reported in the

literature [Hallinan and Elabd. J. Phys. Chem. B. 2007, 111, 13221-13230]. Of the proposed polymer response mechanisms, only one - a reaction-limited, local response to increasing methanol concentration that takes the entire experimental time frame of 600 seconds - produces simulated FTIR-ATR data consistent with experiment. The simulations show that water diffusion out of the membrane is minimal during methanol sorption, and that changes in the measured infrared absorbances are due primarily to the increase in methanol concentration accompanied by dilution of water during swelling. Swelling involves densification of the polymer structure even as there is an overall volume expansion of the film. Potential connections between the polymer densification and molecular-level structural changes of Nafion in methanol are discussed. These results indicate that the interaction between methanol and Nafion serves to increase Nafion's capacity to accommodate large volumes of methanol-water solutions, facilitating increased permeation across the membrane relative to pure water.

Introduction

Polymer electrolyte membranes (PEMs) are widely used in energy conversion devices, e.g., batteries, electrolyzers, and fuel cells.[1-5] In these electrochemical systems, the membrane separates the cathode side from the anode side; ideally its permeation properties allow ions that are needed in the reduction or oxidation reactions to move between the two sides, while simultaneously inhibiting cross-over of product species. The permeability of a PEM is determined by its internal structure. The most well-studied PEM is Nafion, which consists of a poly(tetrafluoroethylene) backbone with sulfonyl fluoride vinyl ether side chains randomly distributed.[6-8] Nafion's conductivity and permeability are determined by the amount of water in

the membrane, which can reach up to 20% by weight or 55% by volume when immersed in liquid water.[6] The sorption of water results in swelling[9] and creates a phase segregated structure, in which the water and ionic sulfonyl group form hydrophilic clusters connected by cylindrical or lamellar channels, and the fluoroethylene backbone forms a separate hydrophobic phase with an average of 10% crystallinity. [6, 10-11] The side chains form an amorphous shell around the water clusters.[12] The size, shape, and distribution of clusters and channels depend on the degree of hydration, the presence of other solvents, and temperature, among other factors.[6] The phase-segregated structure allows Nafion to pass very high current densities but also provides aqueous channels that reduce its ability to block transport of other species that may be present in solution.[13]

Inefficient product-blocking limits the usefulness of PEMs for some applications, especially in low current density devices such as solar fuels generators. Small organic molecules, which are found in liquid fuel cells and photoelectrochemical CO_2 reduction systems, pose a particular problem for product blocking.[14-16] These species tend to interact strongly with the polymer and thus cause changes in its internal structure,[17] which in turn affect their permeation properties. For instance, methanol is an amphiphile whose high permeability in Nafion results in more extensive swelling than in pure water, significant permeant cross-over, and efficiency loss in energy conversion devices. Characterizing molecular-level permeation of PEMs under conditions relevant to their operation in order to learn how to optimize their structure and function remains a challenge. However, the methanol-Nafion system is a useful model for inefficient product blocking, and its study may lead to better understanding of the behavior of

other polymer electrolyte materials in the presence of strongly interacting permeants and of the operation of PEMs in emerging energy technologies.

The internal structure of the methanol-Nafion system is thought to consist of clusters and channels, but with greater disorder than in water-saturated Nafion.[18] As an amphiphile, methanol can interact with both hydrophobic and hydrophilic regions of Nafion and so may reduce the degree of phase segregation.[17, 19] Small angle neutron and x-ray scattering (SANS and SAXS) experiments suggest that methanol sorbs into the amorphous regions of Nafion and also reduces the crystallinity in the hydrophobic region.[17, 19] Methanol is more likely to be found next to the hydrophobic backbone than water,[18] because it can orient its methyl group towards the backbone.[20] These interactions cause the backbone to adopt a greater proportion of trans dihedral angles.[21] Methanol also interacts with the ether oxygen atoms[22] and the carbon atom next to the sulfonate group[23] on the side chain, but the resulting changes in conformation are unclear. Methanol causes a decrease in the Nafion's glass transition temperature, Tg,[22] and an increase in backbone mobility,[24] both of which are plasticization effects.

Much of the understanding of permeation of molecular solutes through PEMs is based on studies under steady-state conditions, while intermittent operation in renewable energy systems is not well-studied. Typically, the permeability, P, of PEMs is quantified using the solution-diffusion model, which is the same model used for non-porous, homogeneous polymers.[2-3] Although PEMs like Nafion are non-uniform at the nanoscopic level, their internal structure may fluctuate at finite temperature,[10, 25-28] providing an effectively homogeneous environment inside the membrane.[1] In this model, P is the product of the solubility, S, and diffusivity, D, (i.e., $P = D \times S$) of a permeant within the bulk of the membrane measured at steady state. Both S and D of

methanol in Nafion, and hence its permeability, depend on its concentration in solution, [$MeOH_{(aq)}$],[1, 3, 6, 29-34] as well as temperature, concentration range, and pre-treatment of the membrane. This means that *S* and *D* are quantities sensitive to the molecular environment although the solution-diffusion model does not include molecular details directly.

To investigate permeation outside of the steady-state regime, we perform kinetics simulations to identify key mechanistic elements and identify where understanding can be improved by theory or further experimentation. The approach we take is to construct multiscale reaction-diffusion models that link molecular-level events to experimental observables using validated kinetic data. The simulations must correctly reproduce a number of time-dependent experimental data using a minimum of assumptions in order to be considered valid. When successful, the calculations provide a full picture of the permeant-membrane system as a function of time that is well-grounded in known physical chemistry, enabling an improved understanding of important physical interactions. The aim of this paper is to build and analyze a model for methanol sorption into hydrated Nafion as a model PEM-permeant system, which is an essential component of the more complex full cross-membrane permeation model that is our ultimate goal. The calculations are compared to observations from an in-depth Fourier transform infrared attenuated total reflectance spectroscopy (FTIR-ATR) study,[1] and provide new information on the contributions of swelling and concentration-dependent diffusion coefficients to the observed transport data. We use the simulations to reinterpret the experimental data in light of these findings and to describe key aspects of the swelling process itself. This new understanding can provide a foundation for the future development of theories for time-dependent membrane permeation.

Model development

An inductive approach to building a sorption model is used herein: the model starts with the simplest possible description of sorption using known kinetics, and details are added only where necessary to quantitatively reproduce experimental measurements.[35] In the present work, validation of the model requires agreement with several data types: the thickness, methanol content, and water content in the initial and final equilibrated states, and the time-resolved relative absorbances of water and methanol. By reproducing all these data with the simplest possible description, the important kinetic contributions to transport into the membrane become clear. Because the experimental data do not include information on the nanoscopic water channels nor the nature of coordination of methanol with Nafion, the averaged bulk description noted above is sufficient. However, as more information becomes known, it is possible to add details of the membrane's internal structure to the existing model to further expand its explanatory power.

The model starts from a previously developed general reaction-diffusion framework for transport of weakly-interacting molecules through a rubbery polymer membrane.[36] In that model, the reactions are the permeants' attachment and detachment at the surface of the polymer. In this study, we extend the framework to include swelling and environment-sensitive diffusion by including additional reactions to describe these changes in the internal polymer environment. Because the influence of swelling and environment on methanol sorption into Nafion have not been characterized, it has been necessary to evaluate a number of mechanistic alternatives (scenarios) to determine which model produces results consistent with experiment. Scenarios that

do not reproduce experimental observations can be ruled out, whereas those that do can be evaluated to gain insights to the underlying physics.

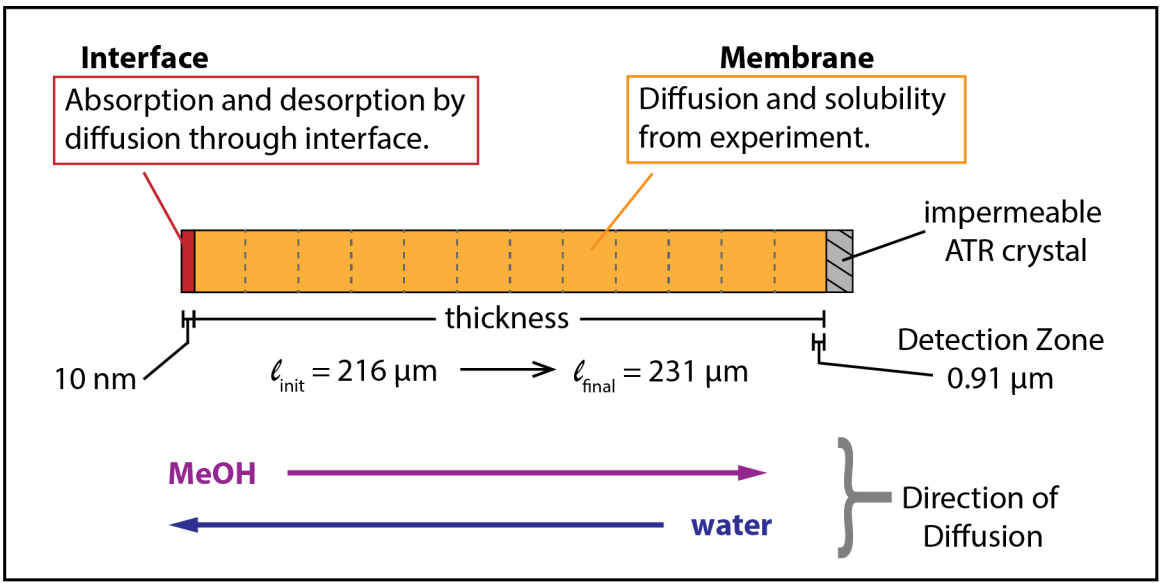

Figure 1. A schematic of the multi-scale reaction-diffusion model (not to scale). The dashed vertical lines in the membrane region indicate that the membrane is subdivided into smaller compartments.

The reaction-diffusion model constructed in this work is simulated using a stochastic algorithm, implemented in the open-access package Kinetiscope.[37] The stochastic method is a type of kinetic Monte Carlo that provides a rigorous solution to the master equation for Markov systems and produces an accurate time base.[38-39] For complex material systems, stochastic methods provide a valuable alternative to coupled differential equation integrators such as those used in finite element methods because they readily accommodate moving boundaries (volume changes) and large ranges in reaction and diffusion rates that change over the course of the

simulation. The simulations generate full spatially resolved data on concentration and volume as a function of time that can be analyzed to predict experimental results, including details at both nano- and macroscopic levels, and provide insights to system characteristics that may be experimentally inaccessible. Further details on computational methodology, along with applications to condensed phase organic and polymeric systems, can be found in previous publications.[36, 40-45]

Synopsis of the experiment. The sorption simulations aim to reproduce time-resolved Fourier transform infrared attenuated total reflectance (FTIR-ATR) spectroscopy data reported by Hallinan and Elabd.[1] A brief synopsis of the experiment is given here so that the correspondence to the multi-scale simulation setup is clear. In particular, the details of the spatial layout and the definition of initial time point (t = 0 s) are important for the proper comparison of experiment and simulation. In the experiment, Nafion 117, with cross-sectional area of 6 cm^2, is prepared by refluxing in peroxide, acid, and ultrapure water, which removes much of the polymer's anisotropy.[46] The prepared Nafion is clamped to the ATR crystal and soaked in ultrapure water for 2 hours prior to starting the experiment, resulting in an initial water-swollen thickness of l_{init} = 216 ± 1 μm. At the start of the experiment (time = 0), an aqueous solution of a specific concentration of methanol, [$MeOH_{(aq)}$], ranging from 1 to 16 mole/L, is pumped into the ATR cell, making contact with the Nafion-solution interface. The pumping rate is assumed to be fast enough to rapidly establish a constant upstream concentration and minimize boundary layer effects. At the Nafion-ATR crystal interface, the changes in water and methanol concentrations are monitored using their unique vibrational spectroscopic signatures. The refractive indices of

the ATR crystal and hydrated Nafion limit the signal penetration depth, d_p, to the 0.91 μm nearest to the crystal. Nafion deposited on solid surfaces has a non-bulk structure that extends ≤ 60 nm from the interface,[46-47] so the majority of Nafion within the detection zone is in the bulk state.

The FTIR-ATR absorbance was shown to be proportional to concentration for water and methanol for the concentration range used in this experiment.[2] The time-resolved data is reported as relative absorbance, $A_{rel}(t)$, defined as

$$A_{rel}^{MeOH}(t) = \frac{A(t) - A_{init}}{A_{final} - A_{init}} \quad (1)$$

for methanol and

$$A_{rel}^{water}(t) = \frac{A(t) - A_{final}}{A_{init} - A_{final}} \quad (2)$$

for water, where $A(t)$ is the absorbance at time t, A_{init} is the initial absorbance and A_{final} is the final absorbance. In this way, $A_{rel}^{MeOH}(t)$ is defined to rise from 0 to 1, and $A_{rel}^{water}(t)$ is defined to fall from 1 to 0, over the experimental time frame of 600 seconds.

Experimental diffusion coefficients for methanol and water are obtained by a least-squares fit to $A_{rel}(t)$, assuming standard Fickian diffusion with constant diffusion coefficient, thickness, and FTIR-ATR signal penetration depth even though swelling occurs. At the end of each experiment, the final membrane thickness, l_{final}, is measured, showing the extent of swelling that results for each methanol concentration. The most comprehensive set of time-resolved data reported is for an aqueous methanol concentration, [$MeOH_{(aq)}$], of 2 mole/L; the equilibrated system data for this case are reported in Table 1. The reported average diffusion coefficients for this concentration are D_{avg}(MeOH) = (2.64 ± 0.11) × 10^{-10} m^2/s and $D_{avg}(H_2O)$ = (4.06 ± 0.56) ×

10^{-10} m^2/s.[1] The diffusion coefficients for the time-resolved data set that is reported for this methanol concentration are slightly different: D_{exp}(MeOH) = 2.75 × 10^{-10} m^2/s and $D_{exp}(H_2O)$ = 3.67 × 10^{-10} m^2/s.[1] Because validation involves direct comparison to experiment, we used these D_{exp} values in the simulations. They differ from the average diffusion coefficients by +2.6% and -9.6%, respectively, but are within one standard deviation.

Table 1. Initial and Final State of the Membrane from Experiment (Ref. [1]) at [$MeOH_{(aq)}$] of 2 mole/L.

	[$MeOH_{(aq)}$]	*S*(MeOH) [a]	[$MeOH_{(p)}$]	[$H_2O_{(p)}$] [b]	*l*
	mole/L	$(mole/L)_{memb}$/ $(mole/L)_{soln}$	mole/L	mole/L	μm
Initial	0	---	---	21.34	216 ± 3
Final	2	1.32	2.64	19.69	231 ± 2

[a] The solubility of methanol in Nafion depends on its aqueous concentration.

[b] The solubility of water in Nafion is 0.385 $(mole/L)_{memb}/(mole/L)_{soln}$ for all concentrations of methanol.

Reaction-diffusion model characteristics. A schematic of the model is shown in Figure 1. The geometry consists of 232 total compartments, 231 for the bulk polymer plus 1 for the liquid-polymer interface. Each compartment contains a homogeneous mixture of Nafion, water, and binding sites for methanol. Initial concentrations are the same in all compartments, and evolve as

sorption proceeds. The bulk polymer compartments have an initial thickness of 0.935 μm that increases to a final thickness of 1.00 μm. A single 10 nm-thick compartment at one end of the array represents the interface between Nafion and the aqueous solution. The compartment at the other end of the array is in contact with the ATR crystal, and is equivalent to the detection zone for the FTIR-ATR measurements. Simulation results are insensitive to compartment thicknesses less than or equal to the signal penetration depth and to any interfacial thickness from 1 to 100 nm, as shown in the Supplemental Information (SI) Section 1. The simulation neglects boundary layer effects at the liquid-Nafion interface, which are thought to be minimal in the experiment due to the selection of conditions. This assumption was tested, and found to be valid due to the insensitivity of the simulation results to the rate of methanol concentration rise in the interfacial region, as reported in the SI Section 2.

In the interfacial region, two processes take place: methanol adsorption from solution, and water desorption from the membrane. Methanol adsorbs by reacting with an available adsorption site, $\mathbf{S}_{ads}$, at the liquid-polymer interface. The concentration, $[\mathbf{S}_{ads}]$, is set to the same initial concentration of available binding sites for methanol as within the bulk polymer, 2.82 mole/L (see below). The adsorption reaction is considered a diffusion-limited encounter between methanol in aqueous phase and an available adsorption site. From the Smoluchowski equation,[48] a second-order rate constant is calculated. For computational efficiency, it is converted to a pseudo-first order reaction in $[\mathbf{S}_{ads}]$ with a constant $[MeOH_{(aq)}] = 2$ mole/L, resulting in the rate constant $k_{ads} = 8 \times 10^6$ s^{-1}. Water desorbs from the membrane into solution by diffusing away from the interface. The rate coefficient is calculated from the time needed to diffuse through the interfacial region, τ, resulting in a first order reaction with rate constant $k_{des} = 1/\tau = 8 \times 10^6$ s^{-1}.

Values and equations used in the calculations of the rate coefficients, as well as other details of the implementation, can be found in the SI Section 3. The simulation results are insensitive to the specific values of absorption and desorption rate constants over several orders of magnitude, as shown in the SI Section 4, indicating that our simulation results are not strongly affected by the assumptions made about these values.

Diffusion of water and methanol occurs between compartments. The experimental diffusion coefficients (see above) are used unless otherwise noted, and these are assumed to include all information about diffusion path tortuosity and other environmental effects. The diffusion between the interface and polymer is assumed to be the same as within the polymer; the simulation results are insensitive to this assumption, as shown in SI Section 5.

The simulations generate concentrations as a function of time and position for all species present in the system, as well as the instantaneous volumes of each compartment. The calculated concentration changes for water and methanol in the compartment adjacent to the ATR crystal are converted to relative IR absorbances and compared directly to the experimental data.

Initial concentrations. The concentration of polymer is considered to be equal to the concentration of sulfonate groups in Nafion 117, which has an equivalent weight (EW) of 1100 grams of dry polymer per mole of $-SO_3H$. In the initial, hydrated state, this gives a polymer concentration of 1.084 mole/L, which decreases to 1.011 mole/L in the final state. Details of this calculation are reported in SI Section 6. At $[MeOH_{aq)}] = 2$ mole/L, the solubility coefficient for methanol in the membrane is 1.32 $(mole/L)_{memb}/(mole/L)_{soln}$, resulting in a final equilibrium concentration of $[MeOH_{(p)}] = 2.64$ mole/L, from Henry's Law ($[MeOH_{(p)}] = S \times [MeOH_{(aq)}]$). The

initial concentration of sites available for methanol sorption is set to 2.82 mole/L in order for the final value to be reached after swelling.

The total initial concentration of water in the membrane is 21.34 mole/L, and the final concentration of water is 19.69 mole/L. These values are calculated from Henry's Law, using the solubility of water in a Nafion membrane, listed in Table 1. In the simulation, the waters that are present in Nafion's final equilibrated state are termed "fixed," and their concentration is recorded separately from that of the waters that diffuse out, termed "mobile." The initial concentration of mobile waters is 0.244 mole/L (1% of the total initial water), calculated from the difference in the amount of water in the initial and final states divided by the initial volume. This leaves the initial fixed water concentration as 21.10 mole/L; this concentration is reduced to its final value due to swelling.

Treatment of swelling and polymer response. The simulation requires that the thickness of each compartment in the membrane be known at each time point in order for the diffusion rate to be correctly calculated from the instantaneous concentration gradients, but only the initial and final thicknesses are reported in Ref. [1]. To include swelling in the simulation, the volume of each compartment must be continuously updated during the simulation using the amount of each species and its partial molar density, where the partial molar density is the inverse of the partial molar volume. In the simulation, swelling is assumed to occur in one dimension only because clamping the edges of the Nafion to the ATR crystal in the experiment should limit swelling to the direction normal to the plane of the interface. If all species in the membrane are assumed to be incompressible, the final thickness of the membrane is 241 μm, much larger than the

experimentally reported value. This indicates that one or more components of the membrane-solute system must become more dense as the methanol diffuses in.

We assume the molar densities of the liquids remain constant at their values for pure liquid, $\rho(MeOH)$ = 24.7 mole/L and $\rho(H_2O)$ = 55.4 mole/L,[49] because they are fairly incompressible. The volume contraction due to non-ideal mixing of water and methanol inside Nafion would reduce the net volume change during swelling by 1.8% (calculation in SI Section 7) and is neglected. Under these assumptions, the polymer partial molar density, $\rho(polymer)$, must change in order to produce the correct initial and final membrane thickness. The initial partial molar density of the polymer in its hydrated state is found to be 1.774 mole/L, and the final value after methanol permeation is 1.880 mole/L, a contraction of 6%. These densities are considered reliable because the final thickness and the water relative absorbance are highly sensitive to them, as shown in the SI Section 8. Although the polymer itself is becoming more dense, and some water is leaving the membrane, the sorption of methanol results in an overall increase in thickness of 7%. In this analysis, changes in polymer partial molar density incorporate the changes in free (void) volume.

The mechanism for this change in polymer partial molar density is unknown, but must be included in the model in order for the kinetics to be correct. Therefore we propose and evaluate three plausible mechanisms for this process:

(a) Concurrent: The change in polymer partial molar density is a local response to the increase of $[MeOH_{(p)}]$, and the rate of response is an upper limit for a diffusion-limited process.

(b) Delayed: The change in polymer partial molar density is a slower local response to the increase of [$MeOH_{(p)}$], and is a reaction-limited process that converts all of the polymer within the experimental time frame.

(c) Synchronized: The change in polymer partial molar density occurs throughout the membrane at as soon as methanol begins to sorb into the aqueous interfacial region, representing a long-range concerted response of the polymer chains.

These three mechanisms will be referred to as *concurrent*, *delayed*, and *synchronized* throughout this work. Their implementation is described in detail in the SI Section 9. In brief, they are meant to represent potential limiting behaviors of polymer relaxation. For the *concurrent* and *delayed* schemes, a physical reaction between methanol and the polymer occurs and changes the polymer partial molar density. For the *synchronized* mechanism, each time methanol enters the Nafion membrane, a force is exerted on the polymer chains due to a volume increase at the aqueous interface. This force triggers a progressive density change in the polymer. All the schemes use estimated rate constants that result in the correct final thickness.

Polymer density-dependent diffusion. In the basic reaction-diffusion scheme, the diffusion coefficients are held constant as the membrane swells, and so any differences in diffusion rates are solely due to the changing compartment thicknesses, which alter local concentration gradients. We also evaluate whether the polymer density change during swelling can alter the local diffusion coefficients for water and methanol.[50] This can be thought of as a concentration-dependent diffusion coefficient, because the polymer partial molar density is dependent on

methanol concentration. We investigate this possibility for two scenarios for an increase in diffusion coefficient as methanol concentration increases, listed in Table 2. The *delayed* polymer response mechanism is used, and when the polymer state changes, D also changes for both methanol and water. Details of the implementation and additional scenarios are described in the SI Section 10.

Table 2. Changes in Diffusion Coefficient for Water and Methanol for the Polymer Relaxation Scenarios.

Scenario	Initial D	Final D
A	D_{exp}	$2\ D_{exp}$
B	$½\ D_{exp}$	D_{exp}

Results

Thickness changes for different polymer response mechanisms. The change in membrane thickness during sorption is shown in Figure 2. If all species are assumed to be incompressible, the final thickness is 241 μm. The correct final thickness of 231 μm is obtained with all three of the polymer response mechanisms, *concurrent*, *delayed*, and *synchronized*, because they each have the same final polymer partial molar density. Though the initial and final thicknesses are the same, it is clear that the time histories are quite distinctive for the three mechanisms. Contour plots showing the time and position dependence of local swelling and the concentrations of densified polymer, methanol, and water for each swelling mechanism are shown in Figures 3 – 5, allowing the thickness *vs* time curves to be more fully interpreted.

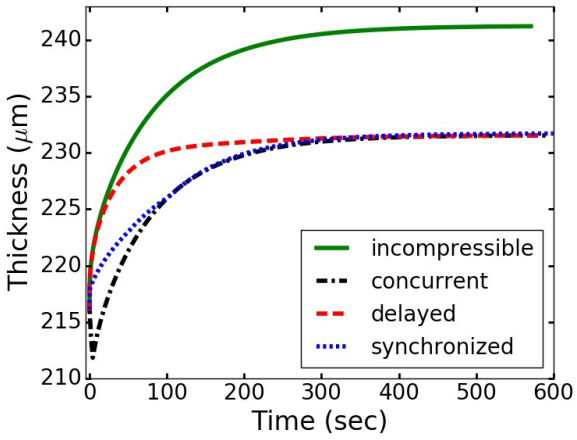

Figure 2. The simulated time-dependent thickness of the membrane compared for the three polymer response mechanisms and a scenario in which all species are incompressible.

Under the *concurrent* mechanism, exposure to the methanol solution leads to an initial, rapid decrease in membrane thickness followed by a smooth increase (Fig. 2). Figure 3 shows that the transient decrease in total thickness (Fig. 3a) is caused by the rapid densification of the polymer (Fig. 3b) in the presence of methanol (Fig. 3c). Even at the Nafion-ATR crystal interface, all the polymer has densified within 5 s although the concentration of methanol is only 0.303 millimole/L. This is because the conversion rate is diffusion-limited, and even a miniscule concentration of methanol triggers polymer densification. The loss of mass due to out-diffusion of water plays a negligible role in this initial thickness contraction: in fact, the reduction in membrane volume causes a concentration increase for water near the Nafion-ATR crystal interface at early times (Fig 3d). Then, as methanol continues to diffuse into the polymer, each compartment in the simulation expands to accommodate the incompressible fluid until the

equilibrium thickness is reached. Expansion of the compartments enables the concentration of methanol to increase while the concentrations of both water and Nafion decrease.

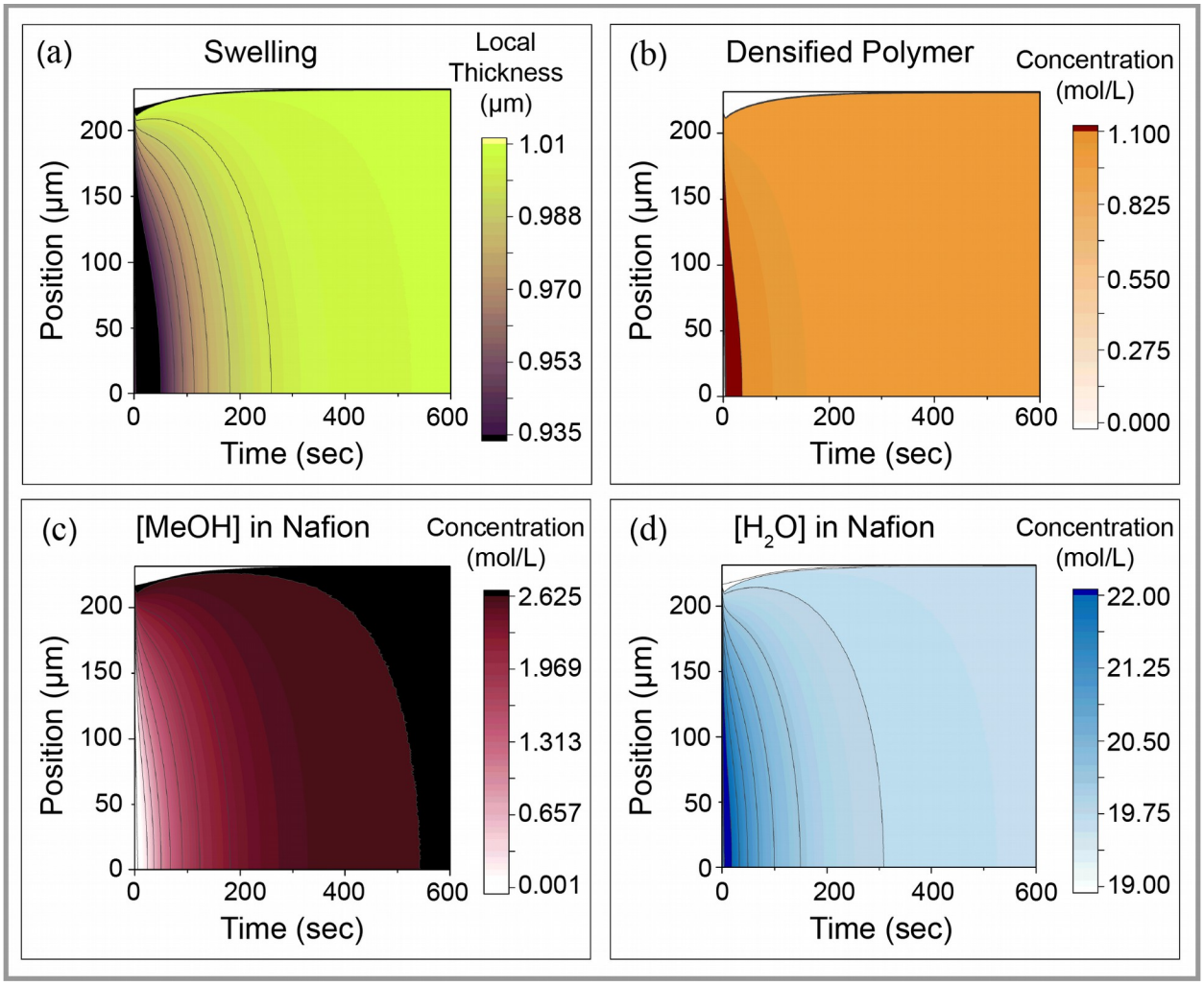

Figure 3. Contour plots for *concurrent* swelling scheme. The (a) thickness (in μm) of each compartment, (b) concentration (mole/L) of densified polymer, (c) concentration (in mole/L) of methanol in the polymer, and (d) concentration (in mole/L) of water in the polymer are shown, as a function of distance from the ATR crystal (y-axis) and time (x-axis). In all of the plots, the position of 0 μm is the interface between Nafion and the ATR crystal, and the maximum position corresponds to the interface between Nafion and the aqueous solution.

The *delayed* swelling mechanism predicts a smooth increase in thickness (Fig. 2); however, this disguises the transient effects that are occurring at the micro-scale. As seen in

Figure 4, because methanol rapidly enters the membrane (Fig. 4c) but the polymer densifies slowly (Fig. 4b), there is a net volume increase of each compartment to a depth of 25 μm from the aqueous interface during the first 200 s of the simulation (Fig 4a). While the polymer in these compartments eventually densifies and their volumes decrease, the methanol concentration increases in the compartments beneath, causing them to swell in turn. The simultaneous polymer densification in one region and compartment expansion with methanol entry in another results in a nearly constant total thickness during the final 400 s of the simulation. The simulations suggest that at the very earliest time, when overall thickness change is minimal, the large volume increase in the solution-Nafion interfacial region results in a compressive force on the film underneath it.

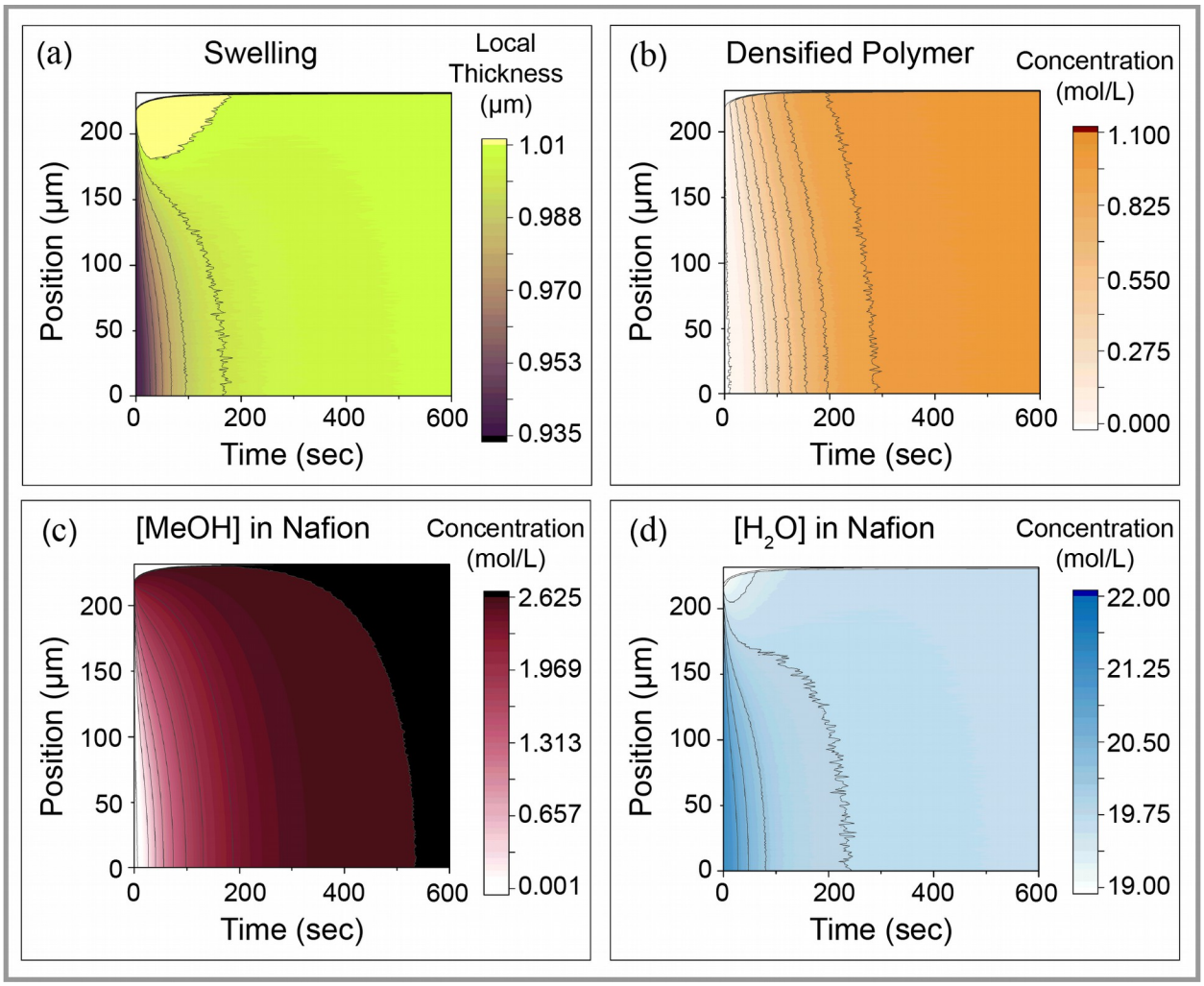

Figure 4. Contour plots for *delayed* swelling scheme The (a) thickness (in μm) of each compartment, (b) concentration (mole/L) of densified polymer, (c) concentration (in mole/L) of methanol in the polymer, and (d) concentration (in mole/L) of water in the polymer are shown, as a function of distance from the ATR crystal (y-axis) and time (x-axis). - In all of the plots, the position of 0 μm is the interface between Nafion and the -ATR crystal, and the maximum position corresponds to the interface between Nafion and the aqueous solution interface.

The *synchronized* mechanism also produces a rapid initial increase in thickness (Fig. 2). Similar to the *delayed* mechanism, rapid in-diffusion of methanol causes swelling at the aqueous-Nafion interface (Fig. 5a). However, this phenomenon occurs in a smaller region, within 15 μm of the aqueous interface, and for a shorter time, only ≈100 s, than in the *delayed* case. As shown

in Figure 5b, the polymer is contracting evenly throughout the membrane, so that the increase in membrane thickness occurs uniformly through the membrane over time.

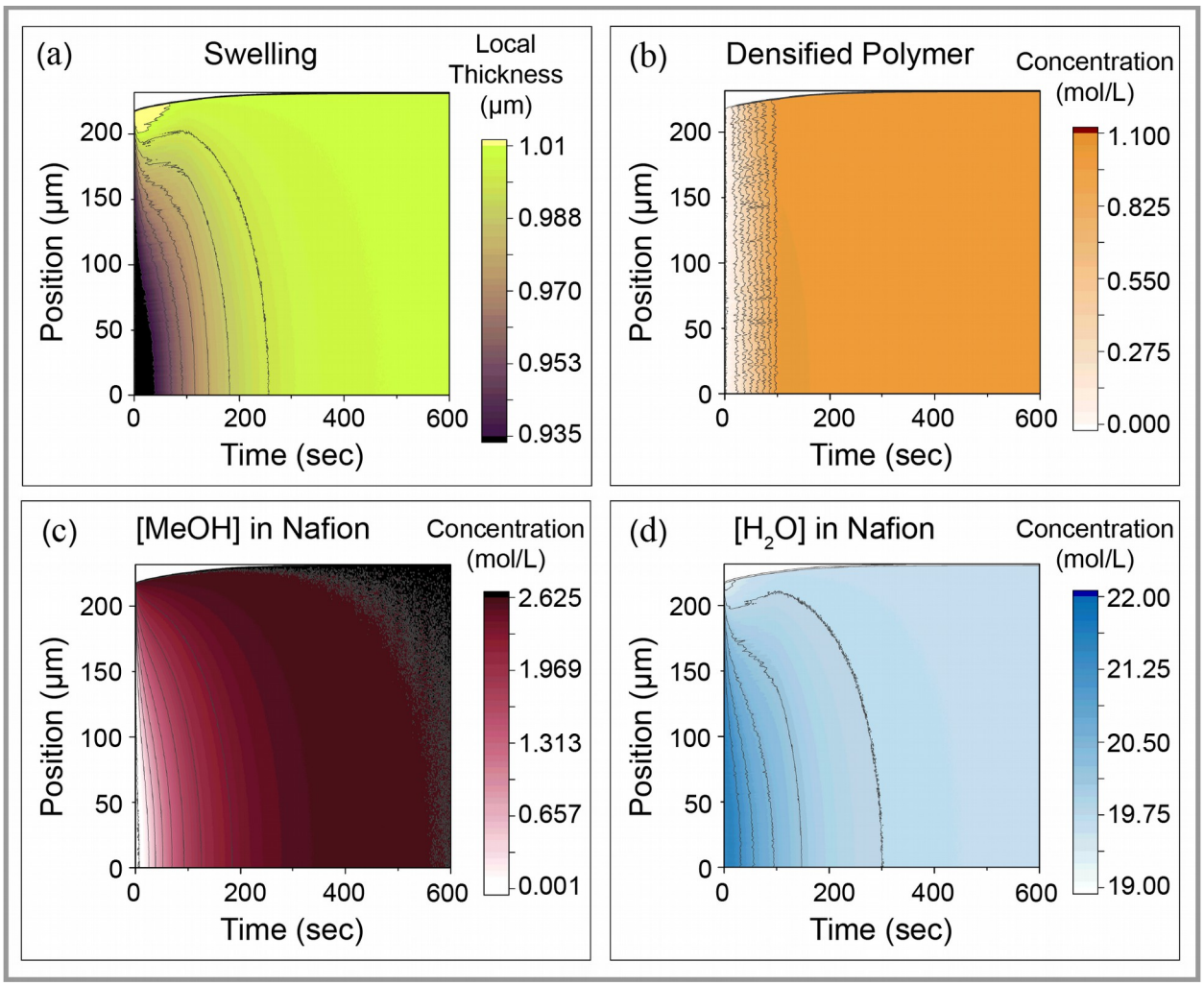

Figure 5. Contour plots for *synchronized* swelling scheme. The (a) thickness (in μm) of each compartment, (b) concentration (mole/L) of densified polymer, (c) concentration (in mole/L) of methanol in the polymer, and (d) concentration (in mole/L) of water in the polymer are shown, as a function of distance from the ATR crystal (y-axis) and time (x-axis). In all of the plots, the position of 0 μm is the interface between Nafion and the ATR crystal, and the maximum position corresponds to the interface between Nafion and the aqueous solution.

Comparison of the contour plots from each mechanism shows that the methanol concentration changes similarly over time and position across the three different mechanisms. The polymer response, shown by the increase in densified polymer concentration, is clearly different between the mechanisms, resulting in differing local degrees of swelling. The summation of local swelling determines the overall thickness at a given time shown in Figure 2. The contour lines in the water concentration profiles most closely resemble the swelling contour lines.

Of particular interest are the concentrations of methanol and polymer within the detection zone of the FTIR-ATR experiment; these are shown in Figure 6 for each polymer response mechanism. Again, a rapid conversion of polymer to its densified state is seen with the *concurrent* mechanism, whereas conversion with the *delayed* and *synchronized* mechanisms are more gradual. In Figure 6c, the intermediate states of the polymer during the *synchronized* polymer response are also shown. The simulation is sampling all of the intermediate states (SI Section 9) at early times, with the final densified state emerging at early time points as well. The concentration of densified polymer in the *synchronized* scheme increases quickly until all the polymer is converted at t = 100 s. In the *concurrent* and *synchronized* schemes, the concentration of the densified polymer decreases after all the polymer is converted due to the increase in volume as methanol continues to enter the detection zone.

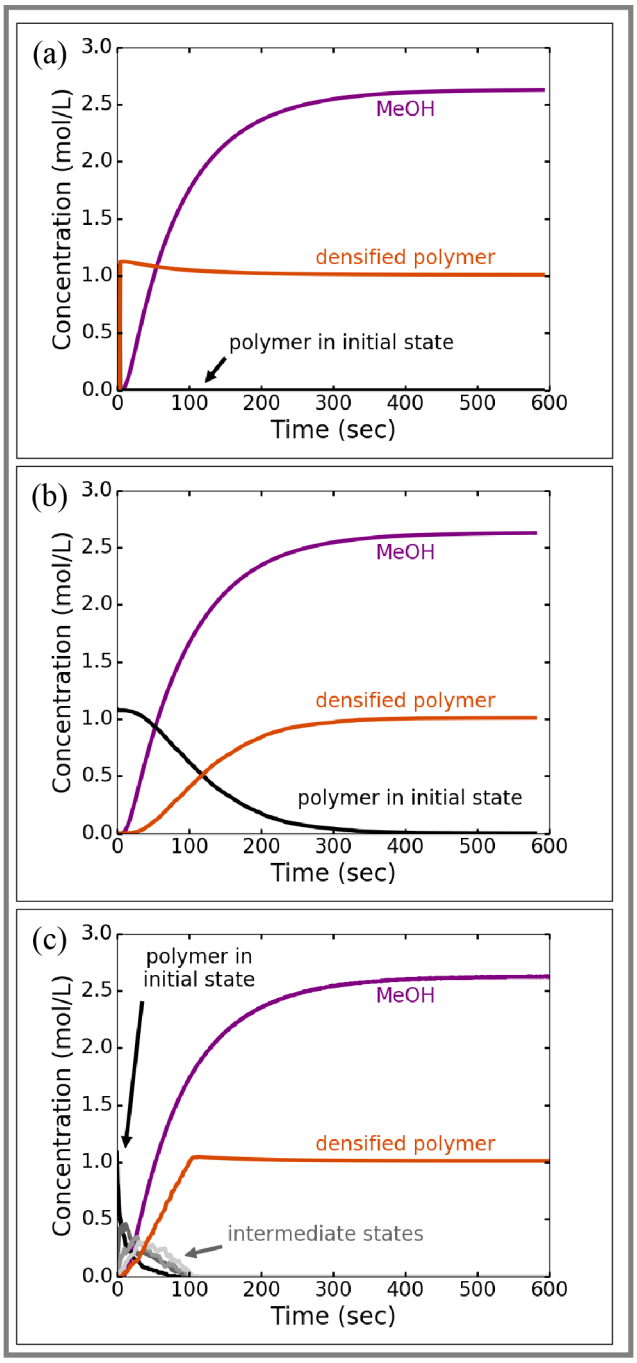

Figure 6. The transition of the polymer from initial to final states in the region closest to the ATR crystal over time, compared to the local concentration of methanol for the (a) *concurrent*, (b) *delayed*, and (c) *synchronized* polymer response schemes.

Predicted FTIR-ATR absorbances for different polymer response mechanisms. The relative absorbances, $A_{rel}(t)$, from the simulation of each polymer response mechanism are shown in Figure 7 and compared to the experimental data. Also included is a curve showing the fit for standard Fickian diffusion using the expression from Hallinan and Elabd,[1] calculated by assuming that the diffusion coefficient, thickness, and signal penetration depth are all constant. It is evident that all simulations and the analytical model give very similar results for the methanol absorbance, but not for water. Both the analytical model and the simulations predict that methanol absorbance increases faster than the observed data at early time points. This may be due to a discrepancy in the definition of the start time (t = 0 s) between the experiment and simulation (discussed in SI Section 2). From t = 12 s to 200 s, there are slight differences between simulated methanol absorbances from the different swelling schemes; these reflect the differences in the concentration gradients created by the different thicknesses as a function of time (Fig. 2), and hence the instantaneous diffusion rates. On the other hand, the water signal calculated from the simulations is very sensitive to the polymer response mechanism. Only the predictions using the *delayed* mechanism are in reasonable agreement with experiment. This indicates that the *delayed* mechanism, in which the polymer densifies throughout the full 600 s (reaction-limited) in response to the local methanol concentration, is the closest of the three mechanisms to describing swelling during sorption in the Nafion-water-methanol system.

The experimental diffusion coefficients are used as a starting point, and the sensitivity of the simulation results to the values of the diffusion coefficients are investigated. A change in the methanol diffusion coefficient of ±20% produces a significant change in both methanol and water absorbance curves. However, the absorbance curves are fairly insensitive to the value of

the water diffusion coefficient. An increase of $D(H_2O)$ by an order of magnitude produces no change at all, though a decrease in $D(H_2O)$ to half its experimentally reported value reduces the rate of absorbance decay of the water. More detail and the absorbance curves for these sensitivity tests are available in SI Section 11.

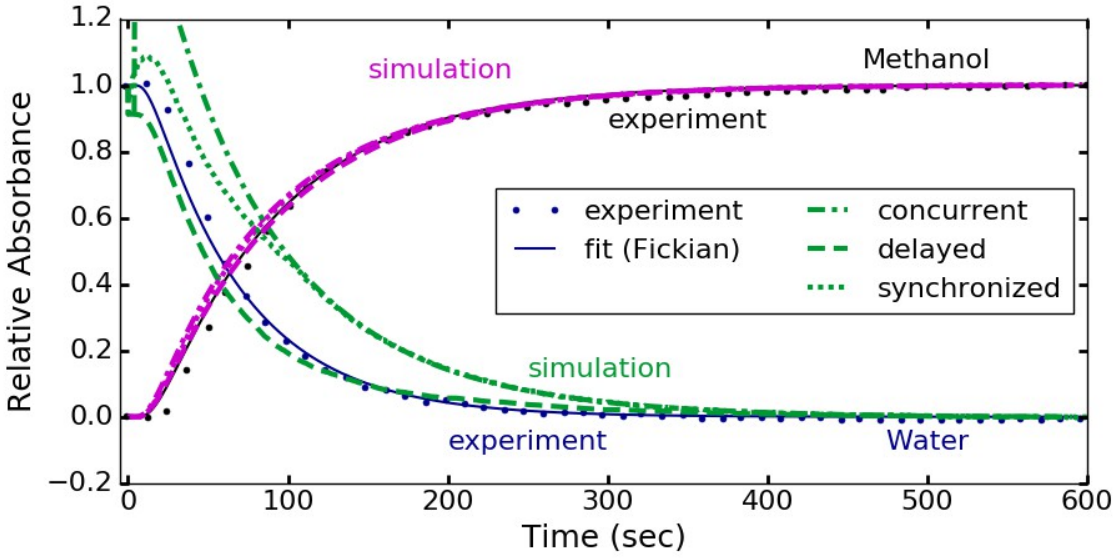

Figure 7. Methanol and water relative absorbance for the three swelling schemes using the experimentally reported diffusion coefficients. Experimental data for methanol are in black and water in blue; the circles are the data points, and the solid line is the fit for Fickian diffusion without swelling. The magenta and green lines are the simulation results for methanol and water, respectively, with the line styles corresponding to different swelling schemes as indicated in the legend.

The concentrations of water and methanol in the detection zone as a function of time and swelling are shown in Figure 8. The mobile water concentration is small at all times, ≤1%, and so as it leaves the film, there is only a slight decrease in total water concentration. The fixed

water concentration is two orders of magnitude greater than the mobile population. Though the amount of fixed water is constant, the increase in volume as a result of methanol entry causes a dilution of the fixed water population. Thus, the decrease in total water concentration is primarily due to swelling, leading to the observed decay in the infrared absorbance. This interpretation is at variance with that proposed in the experimental study, which ascribed the decrease in water absorbance only to out-diffusion.

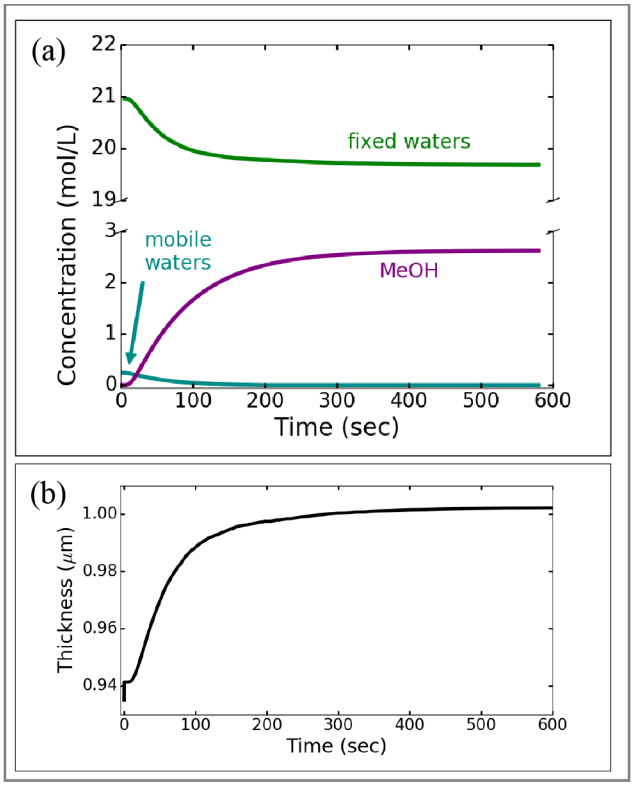

Figure 8. (a) Concentration of methanol and water within the detection zone from simulation of the *delayed* polymer response scheme. Note the scale change on the y-axis. (b) The thickness of the compartment closest to the ATR crystal is shown for comparison.

Predicted FTIR-ATR absorbances assuming polymer relaxation-dependent diffusion. The diffusion coefficients of water and methanol have been reported to depend on methanol concentration. To evaluate whether the diffusion coefficients are sensitive to the local extent of polymer densification, and therefore to the local concentration of methanol, we have allowed D(MeOH) and $D(H_2O)$ to vary using the scenarios summarized in Table 2. The results of the simulations are shown in Figure 9 along with the results from the *delayed* swelling scheme with constant D for comparison.

The absorbances in Scenario A differ greatly from the experimental observations. Conversely, the predicted signals from Scenario B are almost identical to that with a constant diffusion coefficient and with experiment. Together, these results suggest that large changes in the diffusion coefficient (by a factor of 2 or more) during the course of the experiment are possible, but if they occur, the change takes place very early in the permeation process (for the scheme used herein). Thus, the experiment is mainly sensitive to the final diffusion coefficient. This conclusion is further supported by the additional scenarios investigated in SI Section 12.

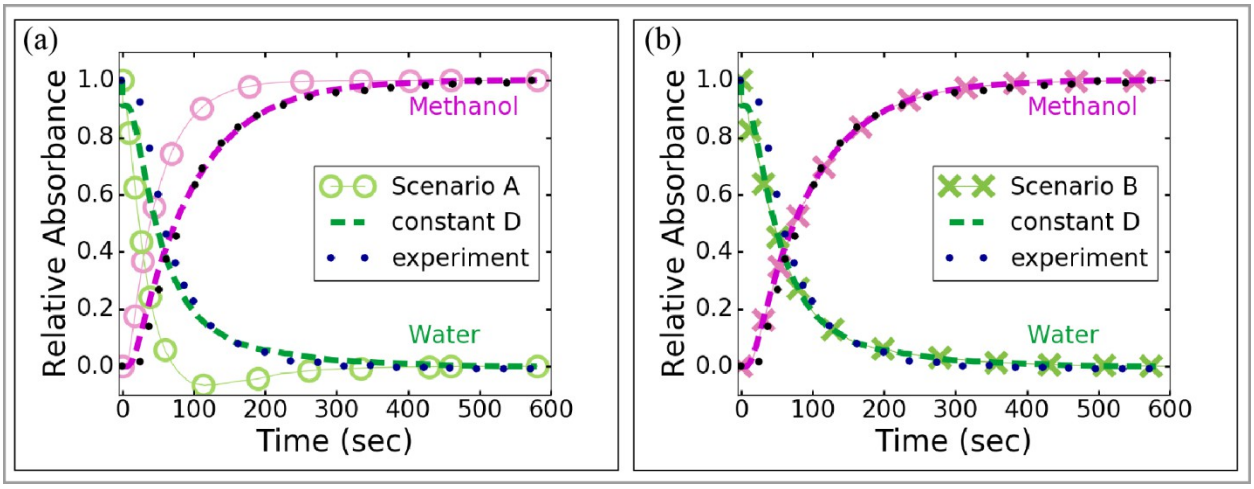

Figure 9. Methanol and water signal for diffusion coefficients dependent on local swelling compared to signals calculated using swelling-independent diffusion coefficients and the *delayed* polymer response scheme for (a) Scenario A and (b) Scenario B. The dashed lines are the results for methanol (purple) and water (dark green) with constant *D* included for comparison. The magenta (methanol) and green (water) symbols are the simulation results for the scenarios indicated on the legend; lines are provided as a guide for the eye. The experimental data for methanol and water are shown by the small black and blue dots, respectively.

Even though Scenario A is known to violate Fickian diffusion in two ways (time-varying diffusion coefficient and thickness), the predicted absorbances can still be fit with the standard analytical solution for Fickian diffusion used in Ref. [1]. For methanol, the overlap between the Fickian fit and the data, shown in Figure 10, is very good. However, the Fickian solution cannot capture the transient reduction in water absorbance below its final value in Scenario A, a feature directly related to swelling. The best-fit values of diffusion coefficients obtained using the Fickian analysis (displayed in Figure 10) are closest to the final diffusion coefficient (see Table S6). For water, the best-fit value is a slight overestimate, and for methanol a slight underestimate. These observations further support the idea that the absorbance curves are sensitive primarily to the final diffusion coefficient (in addition to swelling). This test also demonstrates that the ability of a Fickian model to fit a set of data is not a guarantee that simple Fickian diffusion is occurring.

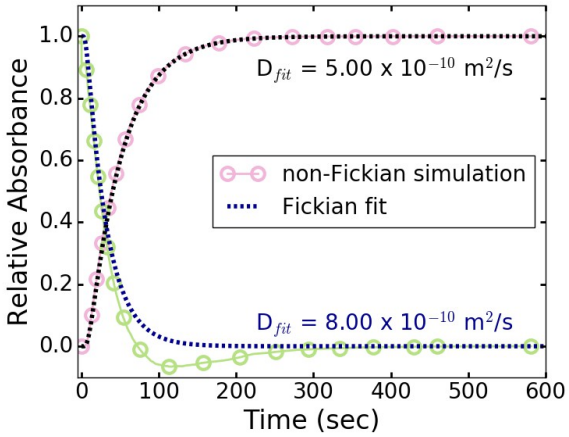

Figure 10. Infrared data calculated by Scenario A and fit with a Fickian diffusion equation.

Simulations of FTIR-ATR data for a range of methanol concentrations. The infrared experiments examined sorption from aqueous methanol solutions ranging from 1 to 16 mole/L. The scheme validated for [$MeOH_{(aq)}$] = 2 mole/L is used to simulate infrared absorbance changes for this range of concentrations. Adjustments made to the reaction-diffusion scheme to account for different degrees of swelling and [$MeOH_{(aq)}$], are described in SI Section 13, and details of the simulation results are presented in SI Section 14. For all concentrations, the simulated and experimental data for equilibrium states are shown in Table 3, and the diffusion data are shown in Table 4. They show that as the methanol concentration increases, there is a progressive increase in swelling, final methanol concentration, and methanol and water diffusion coefficients. The fraction of sorbed water that is mobile also continues to increase, as does the final polymer density.

Plots of the absorbance versus time curves are available in the Figure S14 and are summarized here. For the higher methanol concentrations ([$MeOH_{(aq)}$] = 8 and 16 mole/L), the experimental diffusion coefficients produce good agreement with experimental data. For the

lower concentrations ([$MeOH_{(aq)}$] = 1 and 4 mole/L), the diffusion coefficient of methanol had to be adjusted to obtain the best agreement between experiment and simulation. The best-fit values are higher than the experimentally reported ones and outside of a single standard deviation. The information presented in the experimental study do not allow conclusions to be made about the origin of these differences. In some cases, the simulated water absorbance decay curves display kinks, e.g., Figure S14c. These occur at the time when the last of the mobile water population has left the detection zone, the absorbance decay transitions from a combined diffusion-plus-swelling regime to one solely controlled by swelling. The experimental water absorbance curves are not reported for these concentrations of methanol, and so it is unclear whether these kinks are actually present, or are an artifact of the simulation. Additional experimental data will help answer this question.

Table 3. Summary of equilibrium membrane properties determined from experiment (Ref. [1]) and simulations.

[$MeOH_{(aq)}$]	*l*	swelling [a]	[$MeOH_{(p)}$]	[$H_2O_{(p)}$]	mobile water	[polymer]	ρ(polymer)[b]
mole/L	μm	%	mole/L	mole/L	%	mole/L	mole/L
0 [c]		--	--	21.34	--	1.084	1.774
1	229 ± 5.0	6	1.28	20.50	0	0.865	1.75
2	231 ± 2.4	7	2.64	19.69	1	1.011	1.88
4	235 ± 2.3	9	4.99	18.10	8	0.979	2.10
8	239 ± 1.4	11	8.62	15.59	19	0.992	2.65
16	271 ± 4.6	25	12.8	8.20	52	0.977	2.60

24.6 [d]	270 ± 21	26	14.0	0	100	0.804	2.00 [e]

[a] relative to the pure water swollen state

[b] For comparison, ρ(polymer) = 1.86 mole/L in the dry state.

[c] for Nafion in pure water, equal to the initial state for sorption simulations

[d] Equilibrium-state data are available for this concentration from Ref. [2].

[e] for the average thickness. As a point of comparison, the partial molar density that would produce the maximum thickness (within one standard deviation) of 291 μm is found to be 1.72 mole/L.

Table 4. Summary of diffusion coefficients determined from experiment (Ref. [1]) and simulations.

$[MeOH_{(aq)}]$	*D*(MeOH) sim	*D*(MeOH) exp	*D*(H_2O) exp
mole/L	× 10^{-10} m^2/s	× 10^{-10} m^2/s	× 10^{-10} m^2/s
1	3.13	2.61 ± 0.03	4.15 ± 0.71
2	2.75	2.64 ± 0.11	4.06 ± 0.55
4	4.20	2.80 ± 0.57	4.07 ± 0.56
8	4.32	4.32 ± 0.09	5.63 ± 0.12
16	5.84	5.84 ± 0.04	5.16 ± 0.02

Discussion

The simple multi-scale reaction-diffusion framework constructed in this work is a valuable tool to explain a large amount of experimental data using a simple scheme to represent movement of water and methanol through a polymer. The framework is rooted in the solution-diffusion model, with added elements to include time-dependent polymer densification in contact

with methanol, and overall membrane swelling. This validated sorption model is now extendable to simulate non-steady-state permeation of methanol solutions through Nafion.[3]

It is noteworthy that despite changes in macroscopic and internal structure, the simulations agree with experimental data best when using the experimental diffusion coefficient, which was obtained from a least-squares fit between the experiment and an analytical Fickian equation. This is true even when simulations involve explicit non-Fickian test scenarios, indicating that close agreement between a Fickian analysis and experimental data does not necessarily show that a diffusion process is Fickian. The simulations also show that the diffusion coefficients appear to be essentially constant throughout the polymer contraction and swelling process, although they do vary with methanol concentration in the contacting solution. Tests indicate that if any changes in diffusion coefficients occur, they happen very early in the sorption process so that the experiment is most sensitive to the final value. Experiments that provide more data on early-time diffusion would be needed to determine whether the coefficients in fact do remain constant as the membrane structure changes. The lack of significant concentration-dependence of the methanol diffusion coefficient while the methanol concentration increases in the polymer suggests that the methanol experiences a consistent local environment as it moves through the membrane. Simulation results for water absorbance when $[MeOH_{(aq)}] = 2$ mole/L are very sensitive to the details of the swelling process (Fig. 7), but insensitive to the value of water's diffusion coefficient (Fig. S12) because such a small proportion of water diffuses out of the membrane during methanol sorption, only 1%. The insensitivity of the simulated absorbances to the value of $D(H_2O)$, along with our interpretation that swelling is the origin of the decrease in absorbance, suggest that the diffusion coefficients for water reported for 2 molar methanol may

be rather uncertain. As the aqueous concentration of methanol increases, the proportion of water that diffuses out of the membrane increases. As a result, the simulated water absorbance curve becomes more sensitive to the value of $D(H_2O)$ and the reported values of $D(H_2O)$ should become more reliable at higher methanol concentrations.

It is clear that the polymer partial molar density must decrease during methanol sorption relative to its state in pure water, except when $[MeOH_{(aq)}]$ = 1 mole/L. This increase in Nafion partial molar density is consistent with data from Catalano et al.,[51] in which the water vapor-Nafion system is more dense than expected from additive molar volumes. However, it contradicts a follow-up study by Hallinan and Elabd,[2] in which they report that the density of the methanol-water-Nafion system is lower than expected from additive molar volumes. This inconsistency could reflect differing assumptions about the pure components and the isotropy of swelling, or the accuracy of the experimental measurements of volume. Polymer free volume is not considered separately from the polymer chains in these simulations. Analysis of data from positron annihilation spectroscopy (PALS) implies that there is more free volume, and the voids are larger in an ethanol-Nafion system than in a water-Nafion system.[52] If the same effect is true of methanol or methanol-water mixtures in Nafion, then the polymer packing density would be even greater than estimated here to accommodate the added free volume fraction. However, it is unlikely that the change in polymer partial molar density is solely explained by a change in void volume, since the partial molar density of the polymer dry state and that equilibrated in 2 mole/L of methanol are nearly the same, whereas the partial molar density is lower for the water-only state (see Table 3). This indicates a fairly complex relationship between void volume and permeant content.

A survey of the current literature shows few studies on the molecular-level features of Nafion in methanol and methanol-water mixtures, including structural and kinetic factors, that could lead to the polymer densification required to reproduce the experimental data. Vibrational spectroscopy (FTIR and FT-Raman) indicates that the perfluorinated backbone is coiled in a 15_7 helical conformation (15 backbone units making 7 helical turns) in pure water.[53] Changes in the backbone conformation for methanol-Nafion systems, compared to water-Nafion systems, have been observed small-angle X-ray scattering (SAXS)[19] and molecular dynamics (MD).[21, 24] In SAXS, the presence of methanol is associated with a decrease in Nafion's crystallinity.[19] MD has shown that Nafion backbone segments show a greater preference for trans dihedral angles in the presence of methanol or methanol-water mixtures, compared to pure water.[21, 24] Together, these data suggest that the presence of methanol disrupts the helical structure of Nafion's backbone. Such a change in backbone conformation could be associated with allowing solvent to access regions that had previously been occluded inside of the helix and with greater alignment between the backbones on different polymer chains, which may increase their packing. Either of these options would increase Nafion's polymer chain density even as the whole system swells. A MD study has shown that methanol stiffens the side chain of Nafion while increasing the flexibility of the backbone.[21, 24] Experimentally, methanol reduces the Tg of Nafion,[22] consistent with a greater degree of polymer chain fluctuations, similar to plasticization.

In addition to defining what types of changes occur in Nafion in the presence of methanol, which are steady-state effects, the simulations also provide rate information. The *delayed* mechanism provides a prediction of the rate coefficient for rearrangement of the polymer chains when hydrated Nafion comes into contact with methanol. This rate coefficient is

lowest value for which all of the polymer is converted from its initial to final state within the experimental time frame of 600 s (10 minutes). Studies of the mechanical response of hydrated Nafion are consistent with this timeframe. In a stress relaxation study, Nafion is stretched to a set length, and the force needed to maintain that deformation (strain) is recorded over time.[54] For hydrated Nafion, the stress equilibrates in ≈600 s for a constant strain of 20% and is slower to relax for larger strains.[54] The dimensional change due to swelling in our work is ≤ 25% even for the highest [$MeOH_{(aq)}$], and so a similar or even faster relaxation could be expected. Mechanical studies on the methanol-Nafion system are rare, but a creep compliance test, in which the length of the membrane is observed over time as a constant force is applied, shows a greater degree of deformation occurring over a longer time period than in the water-Nafion system.[55] The data on mechanical properties of Nafion are typically analyzed using the bundle-cluster model to connect deformation to molecular structure changes.[56-57] In this model, tension on the Nafion membrane causes better alignment of polymer backbones within a bundle while increasing spacing between bundles. Such alignment within bundles is another possible structural basis for the increase in polymer partial molar density observed in the simulations herein. Time-resolved mechanical studies may provide an avenue to study polymer chain kinetics during permeation, but further work is needed to connect the observed relaxation times to molecular-level processes.

While the key features of macroscopic transport have been captured with the simple description described herein, as more is discovered experimentally and theoretically about the molecular-level structural and kinetic features of methanol-water-Nafion systems, the details can be incorporated into the multi-scale model in order to elucidate their connections to macroscopic transport and improve the predictive power of the model. For instance, the states of sorbed water

may be extended beyond mobile and fixed to include differences in binding energies to sulfonic acid.[58] The location of the methanol and water can be specified more precisely as being within clusters or in the amorphous regions by including these micro-phases within the polymer phase. Highly spatially- and time-resolved data on swelling will allow the details of the polymer chain density changes to be included and the mechanism proposed in this work to be assessed and validated. Finally, the assumptions concerning methanol absorption into the polymer at the aqueous interface are rather crude, and a more physically realistic description based on additional data from experiment or molecular dynamics simulation would be beneficial. In all cases, the processes and structures would be incorporated via inclusion of new steps in an expanded reaction-diffusion mechanism and definition of a higher resolution geometric grid.

From the present study, some general inferences can be made about modeling methanol sorption into hydrated Nafion, and factors affecting permeability of PEMs in general. The simulations indicate that surface processes are non-rate-limiting as long as the concentration of methanol in the interfacial region is at least as large at its concentration in the bulk of Nafion (SI Sect. 4). The pre-steady-state regime, on the other hand, requires explicit treatment of the swelling mechanism. Therefore, the solution-diffusion model, in which steady-state permeability is the product of S and D, is likely an adequate description only for steady state. Both S and D are large for methanol-water mixtures in Nafion, and increase with increasing methanol concentration.[1] This means that the membrane will become less able to block methanol permeation as the concentration of methanol increases, not only because of the increase in concentration gradient driving diffusion, but also because the intrinsic properties of the membrane are changing. Reports on the reversibility of structural changes in Nafion upon

exposure to methanol are rare.[59] It is possible that methanol exposure can permanently increase Nafion's permeability due to the densification proposed here. Modifications that would reduce solubility of methanol in PEMs have been suggested,[60] including changing the chemical composition such that there is less attraction between methanol and the polymer,[61] and employing chemical cross-linking[62] to improve mechanical resistance to solvent uptake and its associated phase segregation.[63-64] Cross-linking may also decrease diffusivity by increasing the mass of the mobile segment of polymer that controls free volume.[65] Our analysis supports the idea that chemical interaction between polymer and permeant should be reduced in order to decrease solubility and also to prevent structural changes. Both would lead to improved PEM resistance to molecular crossover under operating conditions.

Conclusions

Multi-scale reaction-diffusion simulations of aqueous methanol sorption into hydrated Nafion providing a full time-history of the sorption process are performed and validated with experimental FTIR-ATR data. The sorption process was reported to be accompanied by swelling, however the swelling mechanism and kinetics had not been determined experimentally. The simulations provide insights to this process, and enable the infrared data to be interpreted more fully. Analysis of total swelling data shows that the polymer must become more dense as methanol sorbs into the membrane in order to produce the correct final thickness. Assuming that this is the primary structural change during sorption, three distinct mechanisms for the polymer response to methanol are evaluated. Only one correctly reproduces water infrared absorbance as

a function of time at the polymer-ATR crystal interface: a local, reaction-limited increase in polymer density that accompanies overall swelling in the presence of methanol. The partial molar density increase may be due to a change in packing of the perfluorinated backbone due to interactions between methanol and Nafion's backbone or sidechains. While there is an overall steady increase in membrane thickness during swelling, the simulations predict that the local degree of swelling is spatially and temporally inhomogeneous, a detail that is not probed by the FTIR-ATR measurement. The simulations also enable a more detailed interpretation of the time-dependent infrared data, revealing that the observed decrease in water absorbance during methanol sorption is not due to displacement of water as originally proposed, but due to dilution as the membrane volume increases. It is noteworthy that the diffusion coefficients extracted from the experimental data using a Fickian analysis are accurate even though the film is swelling. The simulations indicate that if changes in the diffusion coefficients occur during the course of the experiment, they are completed early in the sorption process and the diffusant's environment is relatively unchanging past that point. Extension of the simulations to span aqueous methanol concentrations from 1-16 mole/L indicates that the effect of methanol on the internal structure of the membrane is progressive, with increasing polymer contraction and swelling as the external methanol concentration increases. These findings show that reaction-diffusion simulations are a valuable addition to solution-diffusion analysis to gain a more detailed understanding of sorption into polymers on timescales relevant to their operation.

TABLE OF SYMBOLS

Symbol	Units	Meaning

A	---	absorbance
d_p	μm	FTIR-ATR signal penetration depth
D	m^2/s	diffusivity
k_{ads}	s^{-1}	rate coefficient for absorption (pseudo-first order)
k_{des}	s^{-1}	rate coefficient for desorption (first order)
l	μm	thickness
P	m^2/s	permeability
S	$(mole/L)_{memb}/(mole/L)_{soln}$	solubility
t	s	time
ρ	mole/L	partial molar density
τ	s	time for diffusion through the interface
[X]	mole/L	concentration of X
$X_{(aq)}$		X in aqueous phase
$X_{(p)}$		X in polymer phase
$_{init}$		initial state
$_{final}$		final state

ASSOCIATED CONTENT

Supporting Information. The supporting information contains all of the sensitivity studies, reaction schemes, and simulation results for other methanol concentrations. Additional tables of the data in all figures are available at [link to be provided].

AUTHOR INFORMATION

Corresponding Author

* Chemical Sciences Division, Lawrence Berkeley National Laboratory, Berkeley, CA 94720, USA. E-mail address: fahoule@lbl.gov (F.A. Houle).

Author Contributions

The manuscript was written through contributions of both authors. Both authors have given approval to the final version of the manuscript.

ACKNOWLEDGMENTS

The authors would like to thank Dr. Daniel J. Miller for helpful discussions.

Funding Sources

This material is based upon work performed by the Joint Center for Artificial Photosynthesis, a DOE Energy Innovation Hub, supported through the Office of Science of the U.S. Department of Energy under Award Number DE-SC0004993.

REFERENCES

1. Hallinan, D. T.; Elabd, Y. A., Diffusion and Sorption of Methanol and Water in Nafion Using Time-Resolved Fourier Transform Infrared-Attenuated Total Reflectance Spectroscopy. *J. Phys. Chem. B* **2007,** *111* (46), 13221-13230.
2. Hallinan, D. T., Jr.; Elabd, Y. A., Sorption and Diffusion Selectivity. *Mini-Micro Fuel Cells* **2008**, 189-208.
3. Beckingham, B. S.; Lynd, N. A.; Miller, D. J., Monitoring Multicomponent Transport Using in situ ATR FTIR Spectroscopy. *J. Membr. Sci.* **2018,** *550*, 348-356.
4. DeLuca, N. W.; Elabd, Y. A., Polymer Electrolyte Membranes for the Direct Methanol Fuel Cell: A Review. *J. Polym. Sci., Part B: Polym. Phys.* **2006,** *44*, 2201-2225.
5. Lewis, N. S.; Nocera, D. G., Powering the Planet: Chemical Challenges in Solar Energy Utilization. *Proc. Nat. Acad. Sci.* **2006,** *103* (43), 15729 LP-15735.

6. Kusoglu, A.; Weber, A. Z., New Insights into Perfluorinated Sulfonic-Acid Ionomers. *Chem. Rev.* **2016,** *117*, 987-1104.
7. Mauritz, K. A.; Moore, R. B., State of Understanding of Nafion. *Chem. Rev.* **2004,** *104* (10), 4535-4585.
8. Jang, S. S.; Molinero, V.; Tahir, C.; Goddard Iii, W. A., Nanophase Segregation and Transport in Nafion 117 from Molecular Dynamics Simulations: Effect of Monomeric Sequence. *J. Phys. Chem. B* **2004,** *108* (10), 3149-3157.
9. Yi, Y. D.; Bae, Y. C., Swelling Behaviors of Proton Exchange Membranes in Alcohols. *Polym.* **2017,** *130*, 112-123.
10. Allen, F. I.; Comolli, L. R.; Kusoglu, A.; Modestino, M. A.; Minor, A. M.; Weber, A. Z., Morphology of Hydrated As-Cast Nafion Revealed Through Cryo Electron Tomography. *ACS Macro Lett.* **2015,** *4* (1), 1-5.
11. Kreuer, K. D.; Portale, G., A Critical Revision of the Nano-Morphology of Proton Conducting Ionomers and Polyelectrolytes for Fuel Cell Applications. *Adv. Funct. Mater.* **2013,** *23* (43), 5390-5397.
12. Wescott, J. T.; Qi, Y.; Subramanian, L.; Capehart, T. W., Mesoscale Simulation of Morphology in Hydrated Perfluorosulfonic Acid Membranes. *J. Chem. Phys.* **2006,** *124*, 134702-134702.
13. Berger, A.; Segalman, R. a.; Newman, J., Material Requirements for Membrane Separators in a Water-Splitting Photoelectrochemical Cell. *Energy Environ. Sci.* **2014,** *7* (4), 1468-1476.
14. Kuhl, K. P.; Cave, E. R.; Abram, D. N.; Jaramillo, T. F., New Insights into the Electrochemical Reduction of Carbon Dioxide on Metallic Copper Surfaces. *Energy Environ. Sci.* **2012,** *5* (5), 7050-7059.
15. Singh, M. R.; Clark, E. L.; Bell, A. T., Effects of Electrolyte, Catalyst, and Membrane Composition and Operating Conditions on the Performance of Solar-Driven Electrochemical Reduction of Carbon Dioxide. *Phys. Chem. Chem. Phys.* **2015,** *17* (29), 18924-18936.
16. Soloveichik, G. L., Liquid Fuel Cells. *Beilstein J. Nanotechnol.* **2014,** *5*, 1399-1418.
17. Young, S. K.; Trevino, S. F.; Beck Tan, N. C., Small-Angle Neutron Scattering Investigation of Structural Changes in Nafion Membranes Induced by Swelling with Various Solvents. *J. Polym. Sci., Part B: Polym. Phys.* **2002,** *40* (4), 387-400.
18. Kawakami, T.; Shigemoto, I., Molecular Dynamics Studies on the Structures of Polymer Electrolyte Membranes and Diffusion Mechanism of Protons and Small Molecules. *Polym.* **2014,** *55* (24), 6309-6319.
19. Jung, B.; Moon, H. M.; Baroña, G. N. B., Effect of Methanol on Plasticization and Transport Properties of a Perfluorosulfonic Ion-Exchange Membrane. *J. Power Sources* **2011,** *196* (4), 1880-1885.
20. Abroshan, H.; Akbarzadeh, H.; Taherkhani, F.; Parsafar, G., Effect of Water–Methanol Content on the Structure of Nafion in the Sandwich Model and Solvent Dynamics in Nano-channels; A Molecular Dynamics Study. *Mol. Phys.* **2011,** *109* (5), 709-724.
21. Vishnyakov, A.; Neimark, A. V., Molecular Simulation Study of Nafion Membrane Solvation in Water and Methanol. *J. Phys. Chem. B* **2000,** *104* (18), 4471-4478.

22. Martinez-Felipe, A.; Imrie, C. T.; Ribes-Greus, A., Spectroscopic and Thermal Characterization of the Swelling Behavior of Nafion Membranes in Mixtures of Water and Methanol. *J. Appl. Polym. Sci.* **2013,** *127* (1), 246-256.
23. Kumar, K. S. S.; Vijayalakshmi, K. P.; Sivanath, S.; Jayalatha, T.; Mohanty, S.; Shaneeth, M., Interaction of Nafion Ionomers Toward Various Solvents. *J. Appl. Polym. Sci.* **2013,** *128* (6), 3710-3719.
24. Vishnyakov, A.; Neimark, A. V., Molecular Dynamics Simulation of Nafion Oligomer Solvation in Equimolar Methanol-Water Mixture. *J. Phys. Chem. B* **2001,** *105* (32), 7830-7834.
25. Yeo, S. C.; Eisenberg, A., Physical Properties and Supermolecular Structure of Perfluorinated Ion-Containing (Nafion) Polymers. *J. Appl. Polym. Sci.* **1977,** *21* (4), 875-898.
26. Gierke, T. D.; Munn, G. E.; Wilson, F. C., The Morphology in Nafion Perfluorinated Membrane Products, as Determined by Wide- and Small- Angle X-Ray Studies. *J. Polym. Sci.* **1981,** *19* (11), 1687-1704.
27. Page, K. A.; Cable, K. M.; Moore, R. B., Molecular Origins of the Thermal Transitions and Dynamic Mechanical Relaxations in Perfluorosulfonate Ionomers. *Macromol.* **2005,** *38* (15), 6472-6484.
28. Page, K. A.; Park, J. K.; Moore, R. B.; Sakai, V. G., Direct Analysis of the Ion-Hopping Process Associated with the α-Relaxation in Perfluorosulfonate Ionomers Using Quasielastic Neutron Scattering. *Macromol.* **2009,** *42* (7), 2729-2736.
29. Jayakody, J. R. P.; Khalfan, A.; Mananga, E. S.; Greenbaum, S. G.; Dang, T. D.; Mantz, R., NMR Investigation of Water and Methanol Transport in Sulfonated Polyareylenethioethersulfones for Fuel Cell Applications. *J. Power Sources* **2006,** *156* (2), 195-199.
30. Hietala, S.; Maunu, S. L.; Sundholm, F., Sorption and Diffusion of Methanol and Water in PVDF-g-PSSA and Nafion 117 Polymer Electrolyte Membranes. *J. Polym. Sci., Part B: Polym. Phys.* **2000,** *38* (September), 3277-3284.
31. Every, H. A.; Hickner, M. A.; McGrath, J. E.; Zawodzinski, T. A., An NMR Study of Methanol Diffusion in Polymer Electrolyte Fuel Cell Membranes. *J. Membr. Sci.* **2005,** *250* (1-2), 183-188.
32. Ren, X.; Springer, T. E.; Zawodzinski, T. A.; Gottesfeld, S., Methanol Transport Through Nafion Membranes - Electro-osmotic Drag Effects on Potential Step Measurements. *J. Electrochem. Soc.* **2000,** *147* (2), 466-474.
33. Edmondson, C. A.; Fontanella, J. J., Free Volume and Percolation in S-SEBS and Fluorocarbon Proton Conducting Membranes. *Solid State Ionics* **2002,** *152-153*, 355-361.
34. Zawodzinski, T. A., Water Uptake by and Transport Through Nafion® 117 Membranes. *J. Electrochem. Soc.* **1993,** *140* (4), 1041-1041.
35. Bunker, D. L., Simple Kinetic Models from Arrhenius to the Computer. *Chem. Phys.* **1974,** *7*, 195-201.
36. Soniat, M.; Tesfaye, M.; Brooks, D.; Merinov, B.; Goddard III, W. A.; Weber, A. Z.; Houle, F. A., Predictive Simulation of Non-Steady-State Transport of Gases Through Rubbery Polymer Membranes. *Polym.* **2018,** *134*, 125-142.
37. Kinetiscope. http://www.hinsberg.net/kinetiscope/, 2017.

38. Bunker, D. L.; Garrett, B.; Kleindienst, T.; Long, G. S., Discrete Simulation Methods in Combustion Kinetics. *Combust. Flame* **1974,** *23* (3), 373-379.
39. Gillesple, D. T., Exact Stochastic Simulation of Coupled Chemical Reactions. *J. Phys. Chem.* **1977,** *81* (25), 2340-2361.
40. Wallraff, G.; Hutchinson, J.; Hinsberg, W.; Houle, F.; Seidel, P.; Johnson, R.; Oldham, W., Thermal and Acid-Catalyzed Deprotection Kinetics in Candidate Deep Ultraviolet Resist Materials. *J. Vac. Sci. Technol., B* **1994,** *12*, 3857-3857.
41. Houle, F. A.; Hinsberg, W. D.; Morrison, M.; Sanchez, M. I.; Wallraff, G.; Larson, C.; Hoffnagle, J., Determination of Coupled Acid Catalysis-Diffusion Processes in a Positive-Tone Chemically Amplified Photoresist. *J. Vac. Sci. Technol., B* **2000,** *18* (4), 1874-1874.
42. Houle, F. A.; Hinsberg, W. D.; Sanchez, M. I., Kinetic Model for Positive Tone Resist Dissolution and Roughening. *Macromol.* **2002,** *35* (22), 8591-8600.
43. Houle, F. A.; Hinsberg, W. D.; Sanchez, M. I.; Hoffnagle, J. A., Influence of Resist Components on Image Blur in a Patterned Positive-Tone Chemically Amplified Photoresist. *J. Vac. Sci. Technol., B* **2002,** *20* (3), 924-924.
44. Wiegel, A. A.; Wilson, K. R.; Hinsberg, W. D.; Houle, F. A., Stochastic Methods for Aerosol Chemistry: A compact Molecular Description of Functionalization and Fragmentation in the Heterogeneous Oxidation of Squalane Aerosol by OH Radicals. *Phys. Chem. Chem. Phys.* **2015,** *17*, 4398-4411.
45. Wiegel, A. A.; Liu, M.; Hinsberg, W. D.; Wilson, K. R.; Houle, F. A., Diffusive Confinement of Free Radical Intermediates in the OH Radical Oxidation of Semisolid Aerosol. *Phys. Chem. Chem. Phys.* **2017,** *19*, 6814-6830.
46. Kim, M.-H.; Glinka, C. J.; Grot, S. A.; Grot, W. G., SANS Study of the Effects of Water Vapor Sorption on the Nanoscale Structure of Perfluorinated Sulfonic Acid (NAFION) Membranes. *Macromol.* **2006,** *39*, 4775-4787.
47. DeCaluwe, S. C.; Dura, J. A., Finite Thickness Effects on Nafion Water Uptake, Structure, and Ionic Conductivity at Hydrophilic Substrate Interfaces, and Implications for PEMFC Performance. *ECS Trans.* **2017,** *80* (8), 619-632.
48. Keizer, J., Theory of Rapid Bimolecular Reactions in Solution and Membranes. *Acc. Chem. Res.* **1985,** *18* (8), 235-241.
49. McGlashan, M. L.; Williamson, A. G., Isothermal Liquid-Vapor Equilibria for System Methanol-Water. *J. Chem. Eng. Data* **1976,** *21* (2), 196-199.
50. Petropoulos, J.; Sanopoulou, M.; Papadokostaki, K., Beyond Fick: How Best to Deal with Non-Fickian Behavior in a Fickian Spirit. *Diffusion Fundam.* **2009,** *11* (5), 1-21.
51. Catalano, J.; Myezwa, T.; De Angelis, M. G.; Baschetti, M. G.; Sarti, G. C., The Effect of Relative Humidity on the Gas Permeability and Swelling in PFSI Membranes. *Int. J. Hydrogen Energy* **2012,** *37* (7), 6308-6316.
52. Sodaye, H. S.; Pujari, P. K.; Goswami, A.; Manohar, S. B., Probing the Microstructure of Nafion-117 Using Positron Annihilation Spectroscopy. *J. Polym. Sci., Part B: Polym. Phys.* **1997,** *35* (5), 771-776.
53. Di Noto, V.; Gliubizzi, R.; Negro, E.; Vittadello, M.; Pace, G., Hybrid Inorganic-Organic Proton Conducting Membranes Based on Nafion and 5 wt.% of MxOy(M = Ti, Zr, Hf, Ta and

W). Part I. Synthesis, Properties and Vibrational Studies. *Electrochim. Acta* **2007,** *53* (4), 1618-1627.
54. Kusoglu, A.; Tang, Y.; Lugo, M.; Karlsson, A. M.; Santare, M. H.; Cleghorn, S.; Johnson, W. B., Constitutive Response and Mechanical Properties of PFSA Membranes in Liquid Water. *J. Power Sources* **2010,** *195* (2), 483-492.
55. Majsztrik, P. W.; Bocarsly, A. B.; Benziger, J. B., An Instrument for Environmental Control of Vapor Pressure and Temperature for Tensile Creep and Other Mechanical Property Measurements. *Rev. Sci. Instrum.* **2007,** *78* (10), 103904-103904.
56. Liu, D.; Hickner, M. A.; Case, S. W.; Lesko, J. J., Relaxation of Proton Conductivity and Stress in Proton Exchange Membranes Under Strain. *J. Eng. Mater. Technol.* **2006,** *128* (4), 503-503.
57. Rubatat, L.; Gebel, G.; Diat, O., Fibrillar Structure of Nafion: Matching Fourier and Real Space Studies of Corresponding Films and Solutions. *Macromol.* **2004,** *37* (20), 7772-7783.
58. Majsztrik, P.; Bocarsly, A.; Benziger, J., Water Permeation Through Nafion Membranes: The Role of Water Activity. *J. Phys. Chem. B* **2008,** *112* (51), 16280-16289.
59. Umeda, M.; Ojima, H.; Mohamedi, M.; Uchida, I., Methanol Vapor-Induced Morphology and Current – Voltage Characteristic Changes in a Cast-Coated Nafion Film/Interdigitated Microarray Electrode. *J. Polym. Sci., Part B: Polym. Phys.* **2002,** *40*, 1103-1109.
60. Neburchilov, V.; Martin, J.; Wang, H.; Zhang, J., A Review of Polymer Electrolyte Membranes for Direct Methanol Fuel Cells. *J. Power Sources* **2007,** *169* (2), 221-238.
61. Villaluenga, J. P. G.; Barragán, V. M.; Izquierdo-Gil, M. A.; Godino, M. P.; Seoane, B.; Ruiz-Bauzá, C., Comparative Study of Liquid Uptake and Permeation Characteristics of Sulfonated Cation-Exchange Membranes in Water and Methanol. *J. Membr. Sci.* **2008,** *323* (2), 421-427.
62. Chen, L.; Hallinan, J., Daniel T.; Elabd, Y. A.; Hillmyer, M. A., Highly Selective Polymer Electrolyte Membranes from Reactive Block Polymers. *Macromol.* **2009,** *42*, 6075-6085.
63. Diaz, L. A.; Abuin, G. C.; Corti, H. R., Methanol Sorption and Permeability in Nafion and Acid-Doped PBI and ABPBI Membranes. *J. Membr. Sci.* **2012,** *411-412*, 35-44.
64. Fraga, S. C.; Kujawska, A.; Kujawski, W.; Brazinha, C.; Crespo, J. o. G., Transport of Dilute Organics Through Dense Membranes: Assessing Impact on Membrane-Solute Interactions. *J. Membr. Sci.* **2017,** *523*, 346-354.
65. Geise, G. M.; Paul, D. R.; Freeman, B. D., Fundamental Water and Salt Transport Properties of Polymeric Materials. *Prog. Polym. Sci.* **2014,** *39*, 1-42.

TOC Graphic